Penetrative convection in stably stratified fluids[1, 2]

By PETER M. SAUNDERS, *Woods Hole Oceanographic Institution, Mass.*

(Manuscript received October 9, 1961)

ABSTRACT

The downward convection of discrete masses of heavy fluid, called thermals, in a gravitationally stable environment is studied experimentally. For simplicity the ambient stratification is chosen to have a discontinuous two-layer structure with fluid of uniform density in each layer. When released into the homogeneous upper layer the thermal acquires the circulation of a turbulent ring vortex as reported earlier. For weak stratifications, which are however capable of halting the thermal, this circulation is destroyed in a dramatic fashion during the penetration of the lower layer; restoring buoyancy forces then develop a reversed circulation as the thermal flattens and spreads. For strong stratifications no reversal of the circulation occurs, rather the flattening and spreading of the thermal is associated with a gradual decay of the original circulation.

A dimensional argument is proposed to indicate the parameters which determine the extreme penetration of the thermal into the lower layer: this is confirmed by experiment.

In order to generalize the results to more realistic geophysical cases a mechanistic description of thermal behaviour is put forward. The treatment is shown to rationalize the data for environments with (*a*) neutral stratification, (*b*) a discontinuous two-layer structure and (*c*) constant density gradient. Thermal behaviour in a stratification consisting of (*a*) surmounted by (*c*) is then predicted.

Observations made by the author of the penetration of tall cumulus clouds into the sub-tropical stratosphere permit a test of the applicability of this model in one geophysical area. For every 1 km of penetration it is deduced that convective motions have an average vertical intensity of 10 m/sec: this prediction is shown to be in good agreement with the limited observational data.

1. Introduction

SCORER (1957) and WOODWARD (1959) described the convection of discrete isolated masses of buoyant fluid which were introduced into a homogeneous fluid at rest. In this paper an account is given of the behaviour of similar buoyant masses in a fluid with a gravitationally stable stratification of density. The motivation for Scorer's initial study was the concept that atmospheric convection had a discrete unsteady nature and that some of its properties might be revealed by such an experimental study. This view was upheld in a series of observational papers of which the most detailed was by the present author (1961). For the experiments described below the same motivation exists: however, the study can also be shown to have a different and perhaps more general context.

In geophysics we find a number of examples where fluids have a characteristically laminated structure, for example in the terrestrial oceans, atmosphere and liquid core and in stellar atmospheres. In some of these laminations where convection is the dominant transfer process we find the convection bounded by a fluid layer which is the site of other transfer processes (conduction, radiation). In this bounding layer the convective motions are damped out under the action of a stable stratification. Note that the depth that the motions penetrate is the most important single characteristic of this process because material transport and internal waves will occur over depths measured

[1] Contribution No. 1228 from the Woods Hole Oceanographic Institution.

[2] The research reported in this paper was begun during the author's tenure of the Rossby Memorial Fellowship at the Woods Hole Oceanographic Institution.

in terms of this unit. At this time the properties of the penetrative motions are largely unknown and it is hoped that this study will shed light on this important problem.

From an experimental point of view the construction of a well-defined continuous density stratification is not simple, except for example where the gradient can be produced by cooling the bottom and heating the top of a layer of fluid. Since this latter procedure cannot generate a sufficiently large range of density differences for the experiments visualized, it was decided to employ a simple discontinuous stratification, a two-layer structure with a homogeneous layer of light fluid overlying a homogeneous layer of heavy fluid. Such a density structure is reproducible and easy to measure, though not geophysically realistic. However our hope is that armed with a rationalization of the experiments in this simple case we can study other stratifications which are more complex (experimentally) but more realistic (geophysically).

2. Experimental procedure

The experiments were performed in a glass-sided tank with horizontal dimensions 1 m by 1 m filled to a depth of 1.15 m. In the surface layers of the fluid filling this tank heavy convective elements or "thermals" were generated by overturning a hemispheric cup with wall thickness 0.4 mm and capacity 500 cm^3. Here as in the earlier experiments of Scorer and Woodward (loc. cit.) the downward convection of discrete elements is studied: this is a matter of convenience only. For these heavy elements we used salt solutions coloured with fluorescein dye.

The stratification of the ambient fluid was constructed and measured as follows. The tank was approximately half filled with a solution of common salt and water which was stirred vigorously in order to render temperature, salinity and density uniform. After allowing the motions to come to rest fresh water of the same temperature was added above it to form the two-layer structure. Mixing between the fresh and saline fluids was held to a minimum by spreading the fresh water against the underside of a flat wooden board floating in the surface of the fluid. Initially the board floated on the top of the saline layer and the fresh water was introduced slowly: as the thickness of the fresh water layer increased, however, the flow rate could be increased without disturbing the interface. By this method a stratification was generated with the two layers separated by a transition zone where the density changed continuously. Initially the transition zone was approximately 1 cm deep but it was found that this depth could be reduced by slowly sucking out the fluid of the transition zone;[1] using a pipe with orifice diameter 2 mm, 95% of the density change could be concentrated into a layer approximately 5 mm deep. So long as this dimension is small compared with any other characteristic dimension of the experiment we can regard the experimental stratification as a close realisation of the ideal discontinuous structure.

The density of the fluids in the two layers was determined by measuring the apparent weight of the same body immersed in turn in each fluid. A pyrex glass cylinder (having a temperature coefficient of expansion $\frac{1}{20}$ of that of water) with volume 340 cm^3 was employed; it was suspended directly from the arm of a balance by a nylon monofilament and had its long axis horizontal. (This method was developed by J. Richards, Imperial College.) Except for a small correction resulting from changes in the length of the suspending fiber which is immersed in fluid the change in apparent weight divided by the cylinder volume equals the density difference. The method is extremely sensitive; a weight change of 1 milligram corresponds to a density change of approximately 3×10^{-6} gm cm^{-3}.

In the experiments to be described we were not merely content to observe the gross characteristics of thermals (size, position, velocity) but wished also to learn something of the motion field within and without the dense fluid. Because of axial symmetry for this purpose it is necessary to determine the motion in only one diameter plane. Flow visualisation was achieved by employing streak photography on oil particles distributed throughout the fluid in the tank. These particles were mixed from mesitylene ($\varrho = 0.86$ gm cm^{-3}), diethyl phthalate ($\varrho = 1.12$ gm cm^{-3}) and white paint and settled at speeds of 0.5–2.0 mm/sec. The illumination was provided by twelve 300 watt photoflood

[1] This process, which I call "the draining of a stratified fluid", deserves further study.

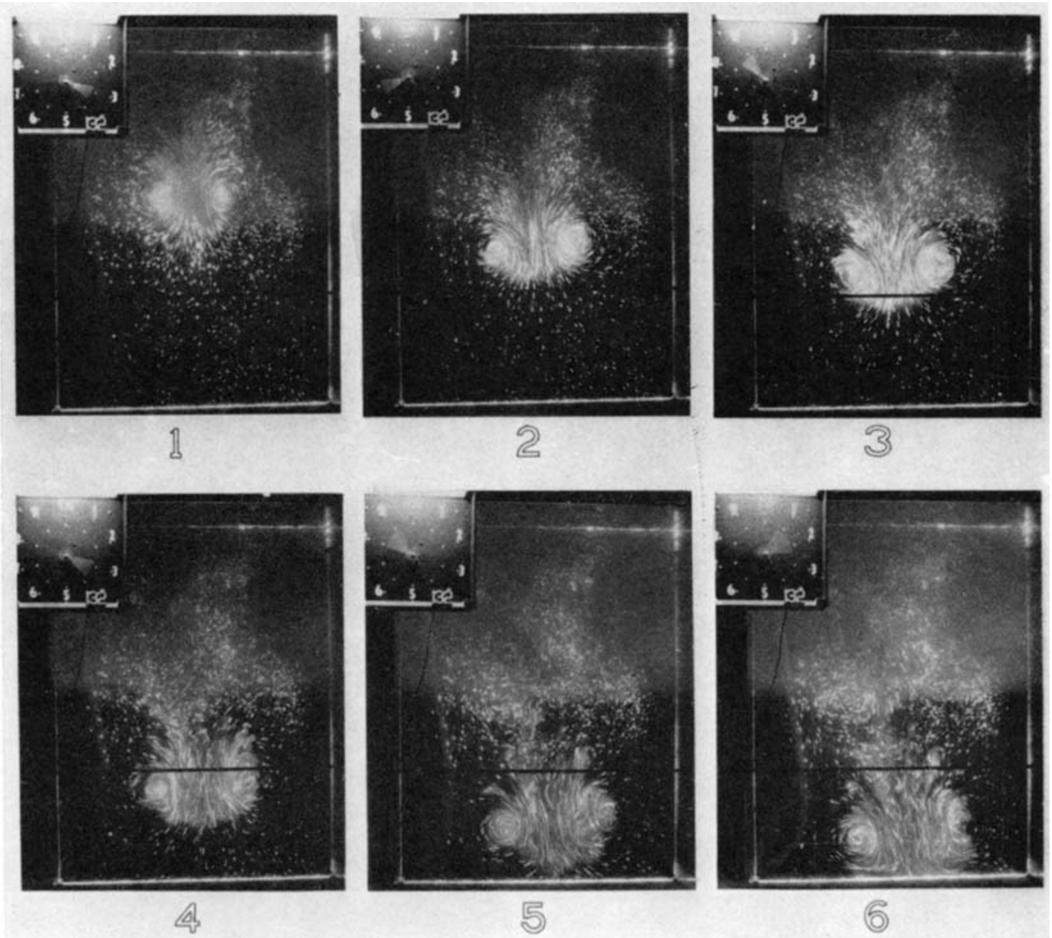

FIG. 1. Streak photographs of thermal behaviour at density discontinuity. Clock indicates time in seconds Exposure of each photo approx. 1 sec. Exp. 132. $\varrho_2 - \varrho_1/\varrho_1 \bar{B}_1 = 0.58$.

bulbs (six per side) shining through an array of vertical slits and producing a curtain of illumination from one wall to the opposite wall and from top to bottom of the tank; the curtain had a thickness of 2 ± 0.5 cm. The thermal was then released so that its axis of symmetry lay in this curtain.

The experients were viewed normal to the curtain of illumination in a darkened room and recorded photographically. A 16 mm ciné camera running at 8 or 12 frames/sec and containing high speed panchromatic film provided the material from which all analysis was made: a 35 mm camera exposed by hand at 2- to 5-second intervals provided the illustrative material (Figs. 1 to 5).

3. Streak photography

Let us first describe the observed fluid motions. In Figs. 1–5 we present the flow fields for five experiments which span a range of values of the parameter $\varrho_2 - \varrho_1/\varrho_1 \bar{B}_1 \cdot \varrho_1, \varrho_2$ are the densities of the fluid in the upper and lower layers respectively, and $\varrho_1 \bar{B}_1$ is the average density excess of the thermal approaching the common interface of the two layers. As we shall establish later, (§ 4) experiments for which the value of this parameter are the same are *similar*.

In the photographs the interface between the layers can generally be discerned either by a change in the opacity of the fluid or by a horizontal line of (white) oil particles. (The dark

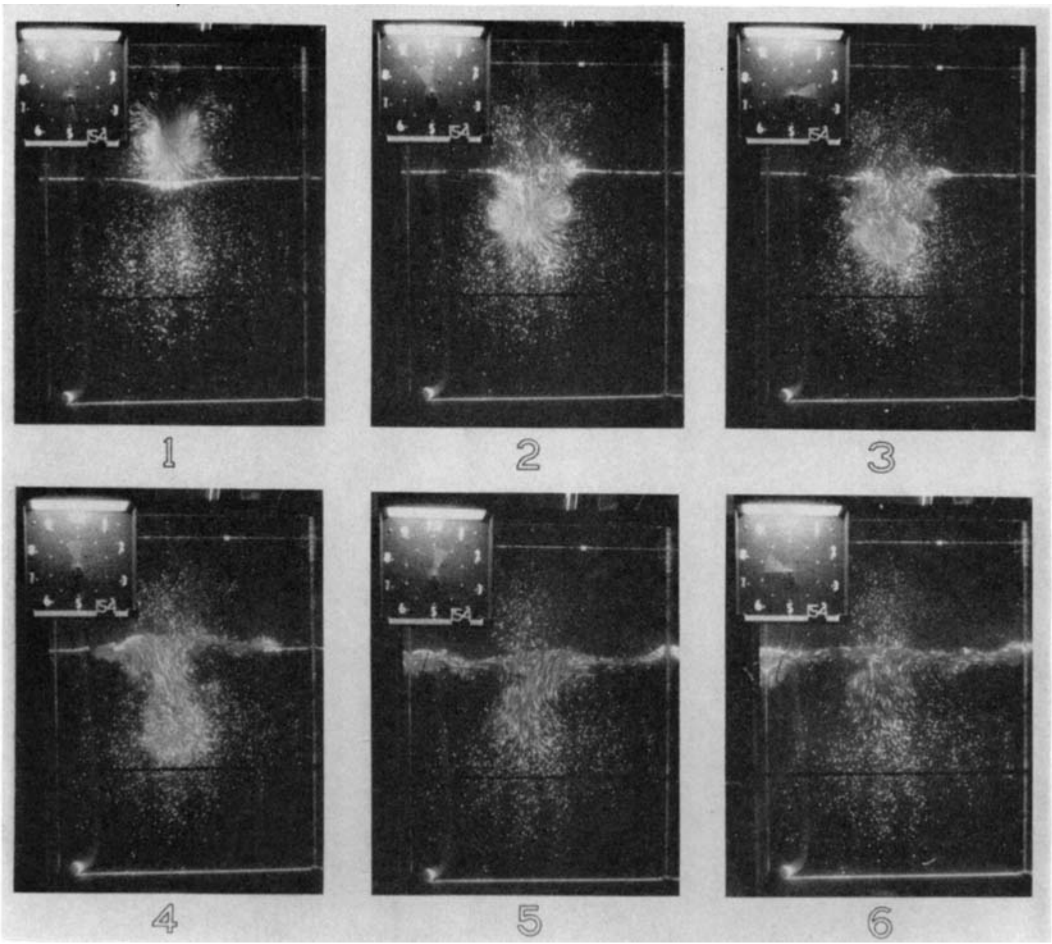

FIG. 2. Exp. 154. See Fig. 1, $\varrho_2 - \varrho_1/\varrho_1 \bar{B}_1 = 0.82$.

line two-thirds of the way down the tank is a structural member.)

It is appropriate to recall that in a neutrally stratified fluid, a thermal advances with fluid in its central core travelling in the same direction but with approximately twice the speed of the leading edge or "cap" of the thermal (WOODWARD, 1959). This statement fixes the sense of the circulation in the early photographs of all the figures shown.

In experiment 132 (Fig. 1), as the thermal passes from the upper layer to the lower most of the fluid of which it is composed remains negatively buoyant; thus the thermal continues to descend until it spreads on the floor of the tank. However a small part of the thermal fluid becomes positively buoyant in the lower layer: this fluid is shed and under the action of its buoyancy generates a weak circulation in the opposite sense to that possessed by the thermal (see photographs 5 and 6). Ultimately this reversed circulation reaches out to the walls of the tank.

In experiment 154 (Fig. 2), in contradistinction to the previous experiment, *all* the fluid of the thermal is positively buoyant in the lower layer. The buoyancy there is small so that under the momentum acquired in the upper layer there is a deep penetration of the lower layer. Note that the thermal retains its vortex-like character (photographs 2 and 3) up to the instant of maximum penetration (photograph 4) when the fluid motion becomes abruptly disordered; the positive buoyancy then sets

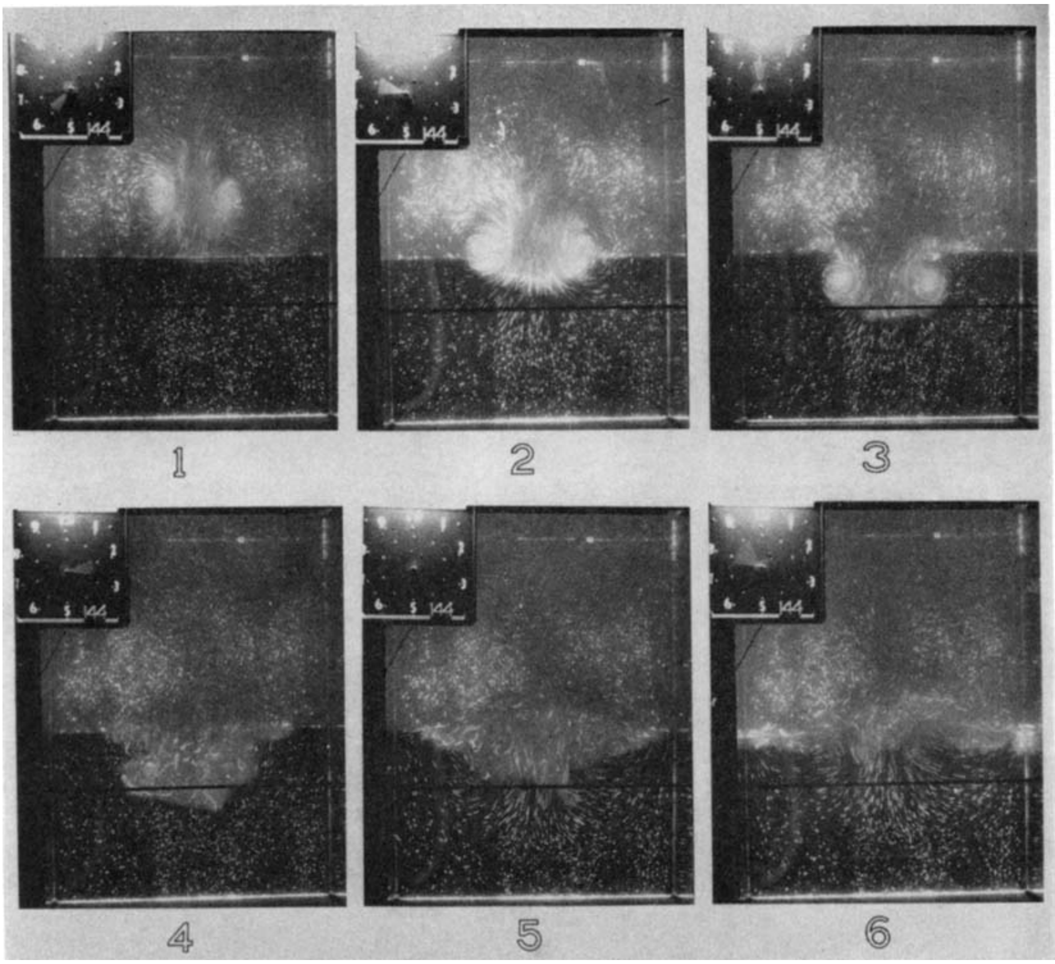

FIG. 3. Exp. 144. See Fig. 1, $\varrho_2 - \varrho_1/\varrho_1 \bar{B}_1 = 1.67$.

up a return flow which is again ordered. Preceding the overall return flow some shedding and the generation of a reversed circulation can be seen.

Because the positive buoyancy of the thermal in the lower layer is greater in experiment 144 (Fig. 3) than previously, its momentum is more rapidly destroyed and its penetration is less. Note again the explosive destruction of the original vortex (photographs 3 and 4) and the generation of an ordered reversed circulation (photographs 5 and 6). This reversed flow has a larger amplitude than previously also because of the larger positive buoyancy force.

In experiments 157 (Fig. 4) and 161 (Fig. 5) the spreading behaviour of the thermal is changed radically. Previously the spreading was associated with a somewhat diffuse circulation having an inward flow in the lower layer and an outward flow in the upper layer; here in experiment 157 the spreading is associated with a more concentrated circulation with inward flow above and outward flow below. This intensification derives from a stretching of vortex lines in the thermal as it approaches the interface of the two fluids (photographs 3, 4, and 5).

(For values of the parameter $\varrho_2 - \varrho_1/\varrho_1 \bar{B}_1$ intermediate between Figs. 3 and 4 there is evidence that two vortices of opposite circulation may appear; one may lie inside the other or one may lie above the other, they are not shown here.)

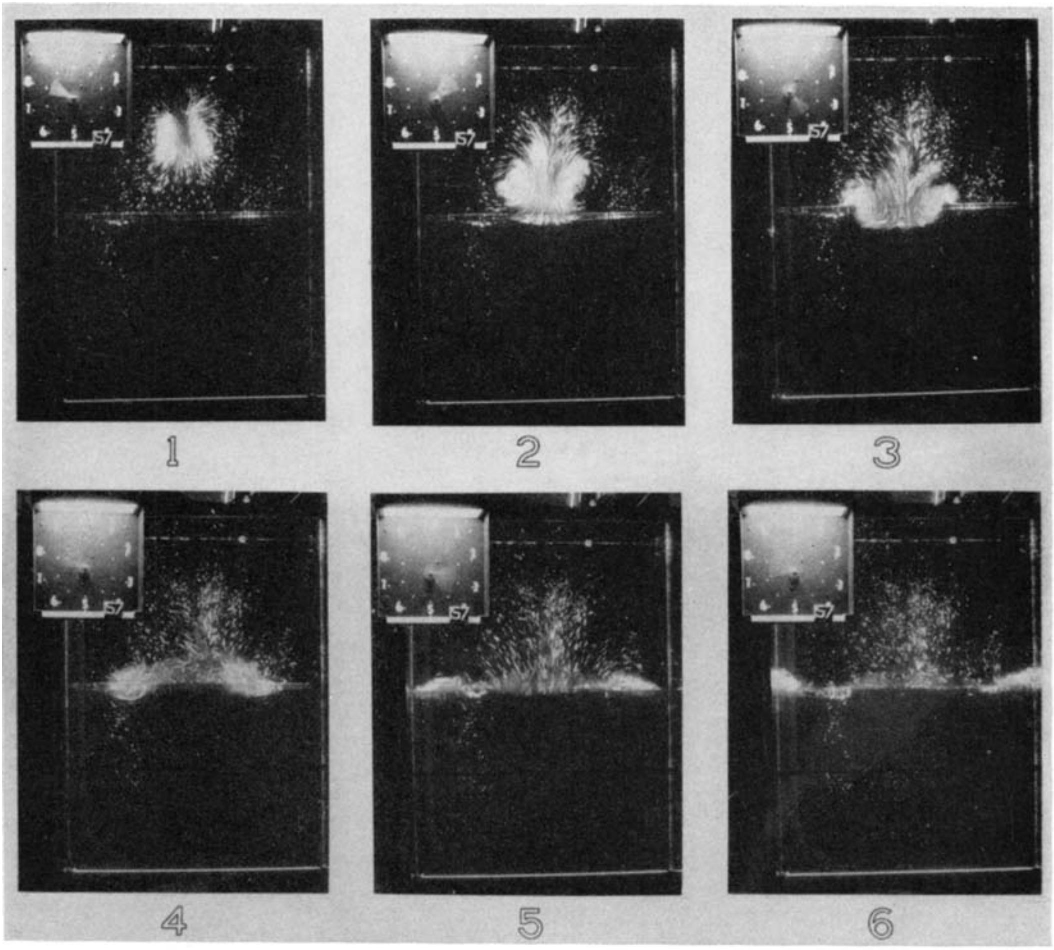

FIG. 4. Exp. 157. See Fig. 1, $\varrho_2 - \varrho_1/\varrho_1 \bar{B}_1 = 5.8$.

In experiment 161 the vortex lines are again stretched in the spreading process: further, be. cause of the great stability of the stratification, there is a minimal distortion of the fluid interface. In this experiment we approximate the behaviour of a thermal approaching a rigid wall with slip.

A partial evaluation of the five preceding experiments will be found in Fig. 6. We have plotted the overall diameter of the thermal D as a function of the height of the cap below the point of release $Z - Z_0$, also the square of the height of the cap measured below the virtual origin of the thermal Z as a function of time t. In the upper layer these pairs of quantities are linearly related (SCORER, 1957); the breakdown of the linearity between Z^2 and t when the thermal enters the lower layer is manifest. Measurements of the diameter after the thermal has reached its peak height are not plotted.

It is evident from the data presented so far that a complete theoretical treatment of the flow is at present beyond our grasp. Nevertheless some important flow characteristics can be deduced from dimensional arguments and because of the simplicity of the method and its relative freedom from specific and questionable assumptions about the flow we present this argument here.

4. A dimensional argument

We shall reckon all heights from the virtual origin of the thermal: Z_1 is then the height of the interface separating the two layers of den-

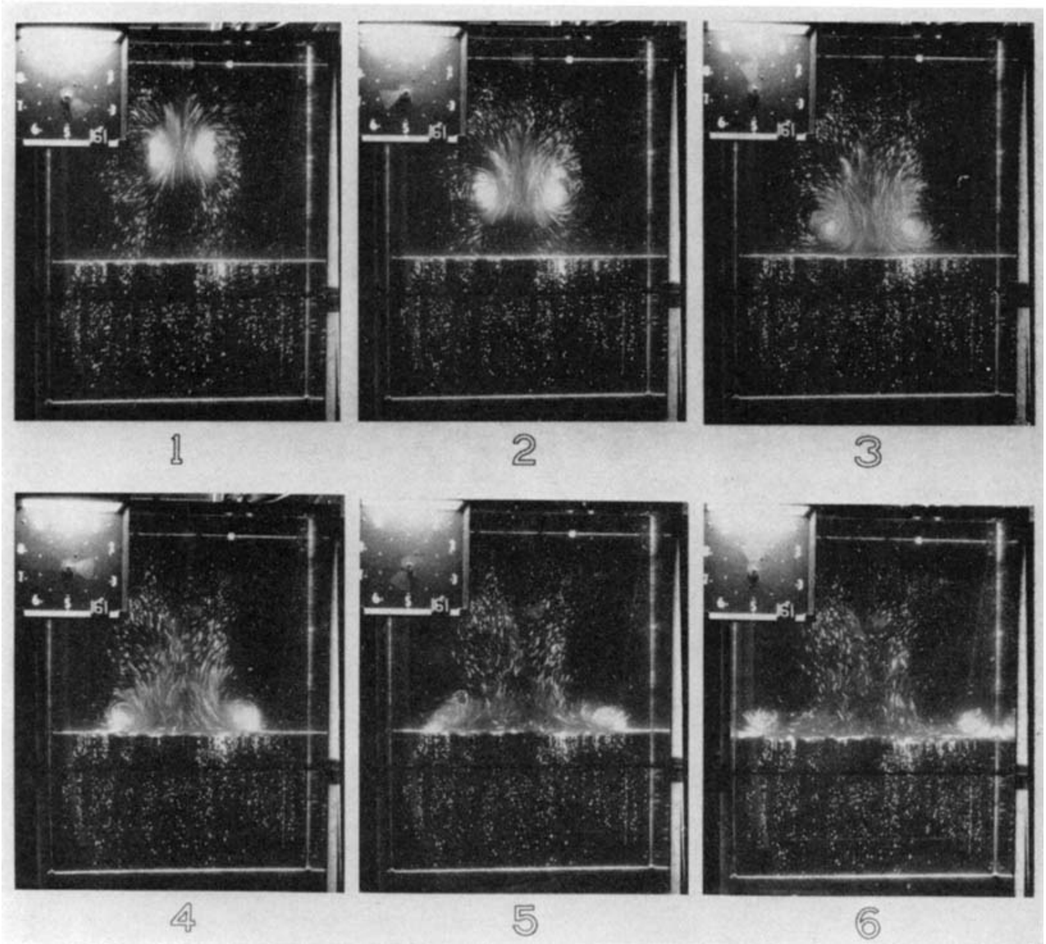

FIG. 5. Exp. 161. See Fig. 1, $\varrho_2 - \varrho_1/\varrho_1 \bar{B}_1 = 26$.

sity ϱ_1, ϱ_2 and Z_P is the peak height that is attained by any fluid of the thermal. We call $Z_P - Z_1 = P$, the *penetration*. Here we shall be primarily concerned with situations where the disposition of densities ϱ_1, ϱ_2, and $\bar{\varrho}$ (where $\bar{\varrho}$ is the volume averaged density of the buoyant fluid of the thermal) is such as to make P finite.

Consider now the physical properties of the system on which the penetration can depend. If we assume that the molecular properties of the fluid do not directly influence the motion, then the complete set is

the dimensions	Z_1 and D_1,
the velocity	W_1,
the buoyancy forces	$g\bar{B}_1$ and $g\bar{B}_2$,

where D_1 is the diameter and W_1 the rate of advance of the cap of the thermal as it approaches the interface; any characteristic length and velocity will serve, these are chosen for convenience. Furthermore the terms $g\bar{B}_1 = g[(\bar{\varrho} - \varrho_1)/\varrho_1]$, and $g\bar{B}_2 = g[(\bar{\varrho} - \varrho_2)/\varrho_2]$ are the buoyant forces exerted on unit mass of a fluid element of density $\bar{\varrho}$ by the upper and lower fluids respectively. Here we employ the familiar argument that density variations appear in the equations of motion only in this combination with gravity g; we thus restrict our arguments to circumstances where the density variations do not appreciably affect the inertia of the fluid. That is $\bar{\varrho}/\varrho_1$, $\bar{\varrho}/\varrho_2$ and hence ϱ_2/ϱ_1 are supposed very close to unity.

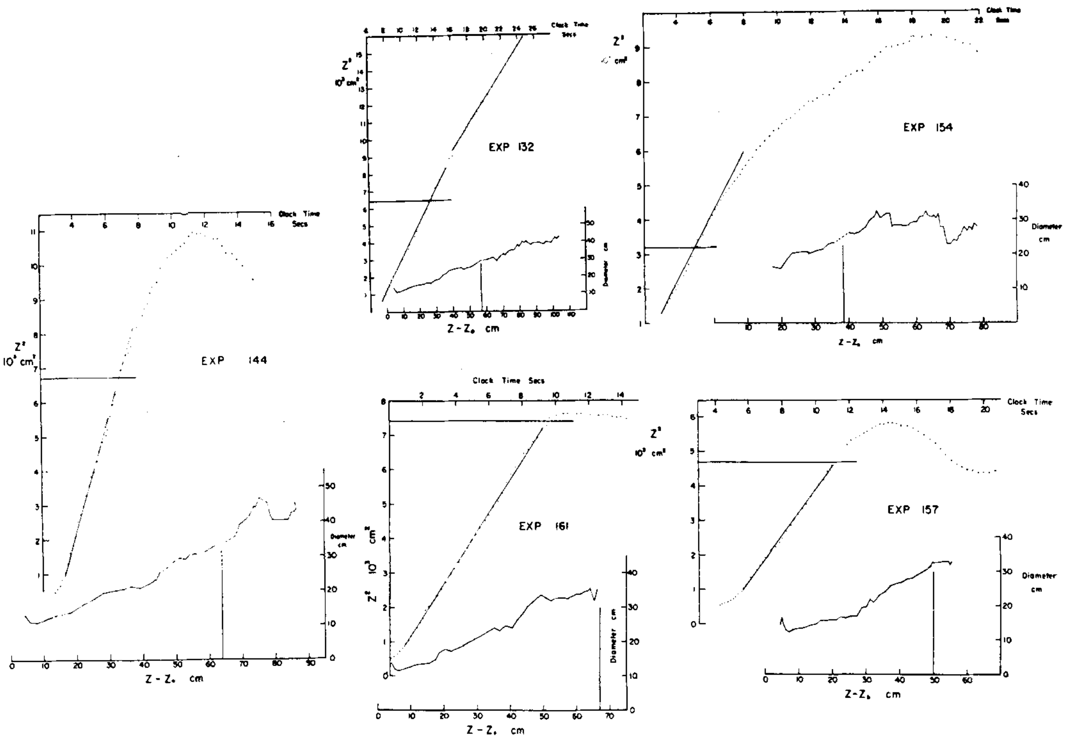

FIG. 6. Height–diameter–time relationships for the experiments of Figs. 1–5.

Forming independent non-dimensional numbers we thus obtain

$$\text{Func}\left[\frac{P}{D_1}, \frac{Z_1}{D_1}, \frac{W_1}{(g\overline{B}_1 Z_1)^{\frac{1}{2}}}, \frac{\overline{B}_2}{\overline{B}_1}\right] = 0.$$

There are of course a number of alternative but equivalent statements of this relationship. Providing we choose to measure D_1 and W_1 (the characteristics of the *approaching* element) at some height close to Z_1, but at a height where the influence of the density structure is not felt, we know from the studies of SCORER (1957) that Z_1/D_1 and $W/[(g\overline{B}_1 Z_1)^{\frac{1}{2}}]$ are constants. (Scorer showed these constants were independent of Reynold's number for the range of values 4000–40,000.) Consequently the functional relationship can be written in the simple form

$$\frac{P}{D_1} = \text{func}\left[\frac{\overline{B}_2}{\overline{B}_1}\right]. \qquad (1)$$

Thus the penetration when scaled by the approach diameter is a function only of the ratio of the (positive) buoyancy force acting on the fluid of the thermal in the lower layer to the (negative) buoyancy force acting on the same fluid in the upper layer.

Because the ratio $\overline{B}_2/\overline{B}_1$ is not measured directly, it is more convenient to use the parameter $\varrho_2 - \varrho_1/\varrho_1\overline{B}_1 \approx 1 - (\overline{B}_2/\overline{B}_1)$. Thus we write

$$\frac{P}{D_1} = \text{func}\left[\frac{\varrho_2 - \varrho_1}{\varrho_1 \overline{B}_1}\right]. \qquad (2)$$

With slight modification to the above argument we may deduce that some characteristic radial spreading velocity of the thermal W_S when scaled by the approach velocity W_1 is a function only of the parameter $\varrho_2 - \varrho_1/\varrho_1\overline{B}_1$, as is also the "time of rise" t when scaled by a characteristic time $\tau_1 = Z_1/W_1$. It is in this sense that we can assert that experiments having the same value for the parameter $\varrho_2 - \varrho_1/\varrho_1\overline{B}_1$ are *similar*. In the following section we attempt to test this conclusion.

5. The experimental data

An examination of the ciné films and streak photographs makes plausible the assertion that up to the time of maximum penetration the fluid motions are not appreciably influenced by the walls of the containing vessel. This assertion can no longer be made about the spreading process where buoyant fluid and internal waves first impinge on the walls and are then reflected by them. Thus in testing the similarity hypothesis we have restricted our attention to relation (2).

For the range of values of $\varrho_2 - \varrho_1/\varrho_1 \bar{B}_1$ encountered, the linearity between Z^2 and t is preserved up to the time when the cap of the thermal reaches the height of the undisturbed interface Z_1 (see Fig. 6). We have thus chosen this instant to measure the "approach values" D_1 and $\bar{B}_1$. Note that the height Z_1 is measured to the centre of the shallow transition zone which separates the two homogeneous layers.

The average buoyancy $\bar{B}_1$ is estimated by computing the volume of the buoyant fluid of the thermal and dividing this into its known weight excess. The volume V is evaluated from an enlargement of the appropriate frame of the ciné film by measuring the illuminated area of the thermal and assuming axial symmetry. For reference the shape factor S of the thermal is then computed from the relation

$$V = S(D/2)^3.$$

Due to the irregular shape of any section of the thermal we estimate that there is an uncertainty in V and hence in $\bar{B}_1$ of up to $\pm 15\%$. This uncertainty generally predominates over all other uncertainties in the experiments and cannot readily be eliminated.

When the density difference between the two layers $\varrho_2 - \varrho_1$ exceeds a value of 2×10^{-2} gm cm^{-3} (over a distance of about 1 cm) we have found that very pronounced refractive effects occur; these make it impossible to measure the penetration of the thermal with any certainty. Since large values of $\varrho_2 - \varrho_1$ are associated with large values of $\varrho_2 - \varrho_1/\varrho_1 \bar{B}_1$ there is an effective upper limit of about 20 on the value of this latter parameter.

Data from 21 experiments is assembled in Table 1 and in Fig. 7 there is a plot of P/D_1 versus $\varrho_2 - \varrho_1/\varrho_1 \bar{B}_1$ which under the similarity

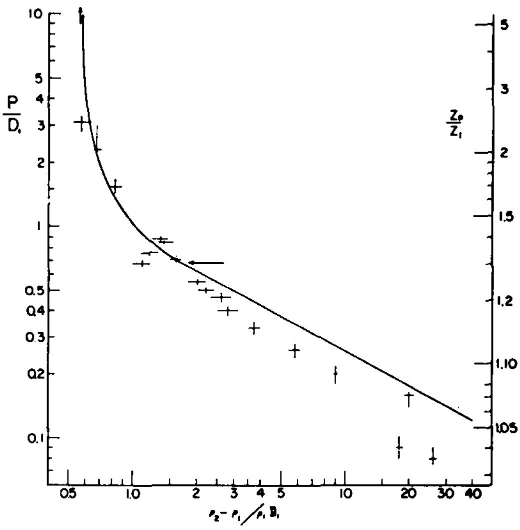

FIG. 7. The penetration of a thermal in a two-layer stratification scaled by its approach diameter and expressed as a function of the parameter $\varrho_2 - \varrho_1/\varrho_1 \bar{B}_1$. The crosses indicate observational points, the continuous line is a theoretical relationship (equations 17).

hypothesis should define a unique curve. Note that whilst the overall range of values of the approach diameter is only 17.5 cm to 38 cm, the approach buoyancy $\bar{B}_1$ varies from 1×10^{-3} to 10×10^{-3}. Experiments 133, 143, 135 and 142 have similar values for both $\varrho_2 - \varrho_1/\varrho_1 \bar{B}_1$ and P/D_1 whilst $\bar{B}_1$ varies by a factor of 6. When we recall that the experiments of Scorer in a neutrally stratified environment showed that the behavior of individual thermals might depart appreciably from an overall norm, for example the rate of increase of diameter with height and the relation between vertical velocity and weight excess varied by up to $\pm 20\%$, we can regard the evidence presented here for the similarity of experiments with the same $\varrho_2 - \varrho_1/\varrho_1 \bar{B}_1$ as strongly confirmatory.

Dimensional argument can tell us nothing further about the nature of the relationship shown in Fig. 7. However in order to extend the usefulness of these experimental results and generalise them to other circumstances we require explicit quantitative relationships. At this stage of development of the subject, we make no apology for the crude mechanistic model of the motions put forward in the following section.

6. A rationalisation of the data

We shall first write down the equations for the model we employ. These are:

A momentum equation

$$W\frac{d}{dZ}(\alpha V W) = g\bar{B}V, \tag{3}$$

A buoyancy equation

$$\frac{d}{dZ}(g\bar{B}V) = -V\frac{g}{\varrho_1}\frac{d\bar{\varrho}_E}{dZ}, \tag{4}$$

A mixing equation

$$V = \beta Z^3. \tag{5}$$

The momentum equation in this form follows from the earlier work of TURNER (1960) in his study of buoyant vortex rings and is

$$\frac{d}{dt}(\alpha W\bar{\varrho}V) = g\bar{B}\varrho_1 V,$$

where W is the rate of advance of the cap of the thermal, $\bar{\varrho}$ is its mean density, V its volume and $\bar{B} = \bar{\varrho} - \bar{\varrho}_E/\varrho_1$ where $\bar{\varrho}_E$ is the volume-averaged density of the fluid displaced, and ϱ_1 is a reference density. α is a virtual mass coefficient and takes into account the dynamics of the fluid which is accelerated around the thermal.

By making a Boussinesq-type assumption, viz. $\bar{\varrho} \approx \varrho_1$ except in the buoyancy term, and noting that

$$\frac{d}{dt} = W\frac{d}{dZ},$$

we derive equation (3).

The buoyancy equation may be regarded as a conservation statement either for heat or for salt depending on the manner in which buoyancy variations arise; for the latter case we have to make the additional assertion that the changes in volume on mixing of fluids are negligible. We can then write down the conservation relation as

$$\frac{d}{dZ}(\bar{\varrho}V) = \bar{\varrho}_E'\frac{dV}{dZ},$$

where $\bar{\varrho}_E'$ is the average density of the fluid entrained into the mass at height Z. We now make the approximation that $\bar{\varrho}_E' = \bar{\varrho}_E$, the average density of the fluid displaced; whence with rearrangement we obtain equation (4).

The third equation is a simple parameterisation of the "mixing" process and is equivalent to the statement that the thermal diameter increases linearly with height. We can justify it by appeal to experiment (see Fig. 6) which shows that up to the time of peak penetration this is a reasonable approximation. Note that it is poorest when the penetration is large but finite. As an alternative formulation of the mixing law was we can assume with MORTON, TAYLOR and TURNER (1956) that the rate of entrainment of exterior fluid into the thermal is proportional to its surface area and rate of advance: equation (5) is then readily shown to follow as a kinematical consequence. We prefer to use the mixing law in the form of equation (5) because it permits a simple integration procedure for equations (3) and (4).

We now propose to explore the properties of these equations by integrating them for various ambient density structures and show how they rationalize a range of experimental data.

CASE (i). NEUTRAL STRATIFICATION

In this case $\bar{\varrho}_E = \varrho_1$ a constant, and equation (4) integrates to give

$$g\bar{B}V = \frac{F}{\varrho_1} = \text{constant},$$

where F is termed the weight excess of the thermal.

Using this relation in the momentum equation (treating α as a constant) we deduce

$$W^2 = \frac{1}{2\alpha}g\bar{B}Z, \tag{6}$$

the form of which result was given previously by SCORER (1957) from dimensional reasoning.

CASE (ii). THE TWO LAYER ENVIRONMENT

In this case a homogeneous layer of density ϱ_1 and depth Z_1 overlies an infinite layer of depth ϱ_2. Now the only region where $\bar{\varrho}_E$ the average density of the fluid displaced by the thermal varies with height is where the thermal is immersed in both layers simultaneously; that is where it lies across the interface between the two layers. If we there approximate $\bar{\varrho}_E$ by the ambient density of the fluid linearly averaged over the vertical depth of the thermal[1] we deduce that

$$\frac{d\bar{\varrho}_E}{dZ}=\frac{\varrho_2-\varrho_1}{h}, \tag{7}$$

where $h=lZ$ is the depth of the thermal.

Hence the conditions on $d\bar{\varrho}_E/dZ$ can be written

$$\left.\begin{aligned}&\frac{d\bar{\varrho}_E}{dZ}=0 \quad (0\leqslant Z\leqslant Z_1 \quad \text{and } Z\geqslant Z_2)\\ &\frac{d\bar{\varrho}_E}{dZ}=\frac{\varrho_2-\varrho_1}{h} \quad (Z_1<Z<Z_2),\end{aligned}\right\} \tag{8}$$

where $\quad Z_2-Z_1=h=lZ_2$

or $$Z_2=Z_1/1-l. \tag{9}$$

Substituting (8) in the buoyancy equation (4) and integrating we obtain

$$\left.\begin{aligned}g\bar{B}V&=\text{const}=F_1/\varrho_1 \quad (0\leqslant Z\leqslant Z_1),\\ &=g\bar{B}_1\bar{V}_1-\frac{g}{\varrho_1}\left(\frac{\varrho_2-\varrho_1}{3l}\right)(V-V_1)\\ &\qquad\qquad (Z_1\leqslant Z\leqslant Z_2),\\ &=\text{const}=F_2/\varrho_1 \quad (Z_2\leqslant Z),\end{aligned}\right\} \tag{10}$$

where F_1 and F_2 are the weight excess of the thermal in the upper and lower layers respectively, and where the suffixes on $\bar{B}$ and V refer to values at height Z_1. Through equation (9), F_1 and F_2 are related according to

$$F_2=F_1[1-\gamma\{(1-l)^{-3}-1\}], \tag{11}$$

where the non-dimensional parameter

$$3l\cdot\gamma=\varrho_2-\varrho_1/\varrho_1\bar{B}_1. \tag{12}$$

[1] This approximation is comparable with that which equates the average density of the entrained fluid to the average density of the fluid displaced. The former may be shown to overestimate the initial decrease of weight excess during penetration, the latter to overestimate it; thus partial compensation occurs. In view of the crudity of the model employed it has not seemed worthwhile to use more exact but more complicated expressions.

The appropriate numerical value for l is 0.23; this corresponds to a flattened volum ewith depth approximately one-half of its diameter. With this value $(1-l)^{-1}=1.3$ and equation (11) becomes

$$F_2=F_1[1-1.2\,\gamma].$$

When $1>1.2\,\gamma$ the weight excess of the thermal travelling in the lower layer has the same sign as it had in the upper layer. Hence the thermal remains heavy in the lower layer and its penetration is infinite. For $1<1.2\gamma$ F_2 and F_1 have the opposite sign so that thermal must be subject to a net restoring force in the lower layer. Consequently penetration is infinite when $\gamma\leqslant 0.83$ but becomes finite for all values of γ greater than this. $\gamma=0.83$ corresponds to a value of $\varrho_2-\varrho_1/\varrho_1\bar{B}_1=0.58$.

Let us now return to the momentum equation: using equation (5), treating α as a constant it is readily transformed to

$$\frac{\alpha}{2}\frac{d}{dZ}(W^2Z^6)=g\bar{B}Z^6.$$

Integrating this equation from height Z_1 where the velocity is W_1 to height Z where the velocity is W we obtain

$$\frac{\alpha}{2}[W^2Z^6-W_1^2Z_1^6]=\int_{Z_1}^{Z}g\bar{B}Z^6dZ.$$

We now transform this equation using the variable

$$\zeta=Z/Z_1 \tag{13}$$

and write $\quad \mu=Z_2/Z_1=(1-l)^{-1}, \quad (14)$

whence $$\left(\frac{W}{W_1}\right)^2\zeta^6-1=4\int_1^{\zeta}\frac{\bar{B}}{\bar{B}_1}\cdot\zeta^6d\zeta, \tag{15}$$

where a group of $W_1Z_1g\bar{B}_1$ and α have been eliminated by equation (6). It is here assumed that not only is α constant, but has the same numerical value[1] as for the neutral stratification. Substituting for $\bar{B}$ from (10) in (15) we can then show

$$\left(\frac{W}{W_1}\right)^2\zeta^6-1=4\left|(1+\gamma)\frac{\eta^4}{4}-\gamma\frac{\eta^7}{7}\right|_1^{\text{smaller of }\zeta\text{ or }\mu}$$
$$+4[1-\gamma(\mu^3-1)]\left|\frac{\eta^4}{4}\right|_{\mu}^{\text{larger of }\mu\text{ or }\zeta} \tag{16}$$

[1] It is not, however, necessary to know this numerical value.

where η is a dummy variable. The integral limits are self-explanatory; note that for $\zeta \leqslant \mu$ the second term vanishes.

(a) Penetration

Let us now calculate the peak height reached by the foremost part of the thermal; put $\zeta = \zeta_p$ and $W = 0$ in equation (16). Then

$$\left.\begin{aligned} \gamma &= \tfrac{1}{4}\zeta_p^4\{\tfrac{1}{7}(\zeta_p^7-1)-\tfrac{1}{4}(\zeta_p^4-1)\}^{-1} \quad (\zeta_p \leqslant \mu), \\ &= \tfrac{1}{4}\zeta_p^4\{\tfrac{1}{7}(\mu^7-1)-\tfrac{1}{4}(\mu^4-1) \\ &\quad + \frac{\mu^3-1}{4}[\zeta_p^4-\mu^4]\}^{-1} \quad (\zeta_p \geqslant \mu). \end{aligned}\right\} \tag{17}$$

Note that when μ is specified (we take $\mu = 1.3$) ζ_ϱ is a function only of γ. Since

$$\zeta_p - 1 = \frac{P}{Z_1} = m \cdot \frac{P}{D_1} \tag{18}$$

where $D_1 = mZ_1$, we immediately see that this statement is equivalent to the result derived from the dimensional argument, namely P/D_1 is a function of $\varrho_2 - \varrho_1/\varrho_1 \bar{B}_1$ only.

In Fig. 7 we have plotted the curve represented by equation (17), and we see that there is reasonable agreement with the experimental results reported earlier. Note that for large values of $\varrho_2 - \varrho_1/\varrho_1 \bar{B}_1$ equation (17) predicts a systematically larger penetration than is observed; a likely explanation is that the virtual mass coefficient α has been overestimated. In circumstances of large $\varrho_2 - \varrho_1/\varrho_1 \bar{B}_1$ as a thermal approaches the interface between the two layers of fluid the motion ahead of it is strongly damped out (compare Figs. 1 and 6); α thereby diminishes. Since for smaller α the same decelerating buoyancy force will halt a thermal within a shorter distance, by reducing α (but maintaining $\alpha > 1$) we can improve the agreement in Fig. 7. However we have not considered the improvement significant and the α appropriate to neutral stratification (equation (6)) has been used throughout this treatment.

(b) Velocity decay

This model of the thermal also permits us to make a test of the height-time relationship for the thermal: writing the right-hand side of equation (16) as $Q(\zeta, \gamma)$ we then have

$$\frac{W}{W_1} = \zeta^{-3}\sqrt{1 + Q(\zeta, \gamma)}.$$

Now $$W = \frac{dZ}{dt} = Z_1 \frac{d\zeta}{dt}$$

and defining $$\tau = Z_1 / W_1$$

we can integrate the equation above to give the time t at which the thermal reaches the height ζ as

$$\frac{t - t_1}{\tau} = \int_1^\zeta \frac{\eta^3}{\sqrt{1 + Q(\eta, \gamma)}} d\eta, \tag{19}$$

where $t = t_1$ when $W = W_1$, $Z = Z_1$ and $\zeta = 1$. The scale time τ can be shown to be twice the time required for the thermal to reach the height Z_1.

In general the form of $Q(\eta, \gamma)$ does not permit us to integrate equation (19) analytically so we have made a numerical integration for three simple cases. We chose $\gamma = 1.18$, 2.41 and 8.58 which are values appropriate to experiments 154, 144 and 157; their height–time plots are shown in Fig. 8. For convenience in presenting them together we have taken as height ordinate $Z - Z_1/Z_P - Z_1$ which varies between 0 and 1 in all cases. As in Fig. 7 agreement is fair.

It is worth recalling that the success we have attained in this treatment stops once the thermal reaches its peak penetration. Thereafter we have no mixing law and because of the flattening and distortion of the thermal the form of the momentum equation can be expected to be changed.

CASE (iii). CONSTANT STABILITY THROUGHOUT

The case of a thermal released into an infinite layer of constant positive stability ($d\varrho/dz$ = constant) was considered by MORTON, TAYLOR & TURNER (1956). Their equations are similar to the set employed here insofar as they deduce the same functional relationships between diameter and height, height and time, penetration and stability (not described here). However in their experiments they observed only the ultimate height at which the thermal came to rest: this cannot be predicted from equations (3) to (5) with certainty. Furthermore because the virtual origin of the thermal was not known the numerical coefficients in the various relations are also not free from uncertainty. Thus though we cannot test the precise numerical predictions of this model here, the predicted

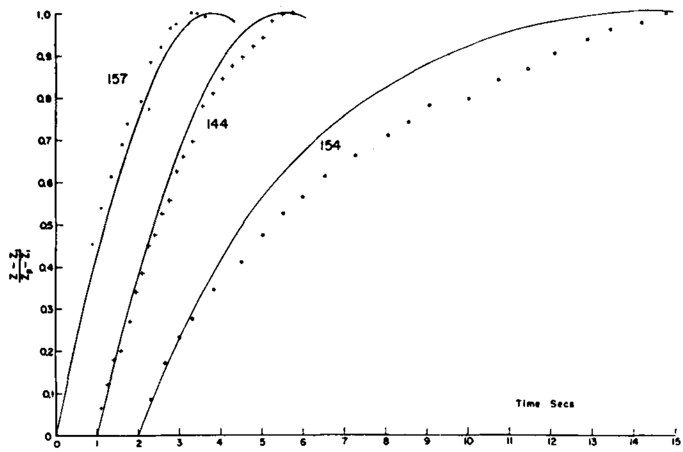

FIG. 8. The height–time relationship for the three experiments of Figs. 2–4.

functional relationships are confirmed by the experimental results.

As a result of the quantitative agreement between the predictions of equations (3) to (5) and experiment in the cases so far considered, we can now proceed with some confidence to treat a stratification for which no experimental data is known to the author.

CASE (iv). A NEUTRALLY STABLE LAYER SURMOUNTED BY A LAYER OF CONSTANT STABILITY

Here we have

$$\varrho_1 = \text{constant} \quad (0 \leqslant Z \leqslant Z_1),$$

$$\frac{g}{\varrho_1}\frac{d\varrho_E}{dZ} = G = \text{constant} \quad (Z_1 < Z).$$

As in case (i) for total immersion of the thermal in the homogeneous fluid $d\bar{\varrho}_E/dZ = 0$. For total immersion in the layer of constant stability we have

$$\frac{d\bar{\varrho}_E}{dZ} = \frac{\varrho_1}{g}G(1 - l/2), \tag{20}$$

where the factor $(1 - l/2)$ arises as follows. $d\bar{\varrho}_E/dZ$ is the change in average density of the fluid displaced per unit advance of the cap: this is also the change in the ambient fluid density at the height of the centre of mass of the thermal per unit advance of the cap. Now unit advance of cap results in a displacement of $1 - l/2$ in the centre of mass. Whence the factor appears in equation (20).

Again as in Case (i) we have a transition zone where the average density of the fluid displaced changes from the value ϱ_1 to the value given by integrating (20): here $\bar{\varrho}_E$ is obtained by taking the linear average of the ambient density for the range of heights occupied by the thermal. We may then show

$$\frac{d\bar{\varrho}_E}{dZ} = \frac{\varrho_1}{g}\frac{G}{2l}\left(1 - \frac{Z_1^2}{Z}\right)$$

where lZ is the vertical depth of the thermal (as in equation (7)). Assembling results the analogue of equations (8) are

$$\frac{d\bar{\varrho}_E}{dZ}\begin{cases} = 0 & (0 \leqslant Z \leqslant Z_1), \\ = \dfrac{\varrho_1 G}{g2l}\left(1 - \dfrac{Z_1^2}{Z^2}\right) & (Z_1 \leqslant Z \leqslant Z_2), \\ = \dfrac{\varrho_1 G}{g}(1 - l/2) & (Z_2 \leqslant Z), \end{cases} \tag{21}$$

where $Z_2 = Z_1/1 - l$ as before in equation (9).

Integrating the buoyancy equation (4) using (21) and (5) we obtain

$$g\bar{B}V\begin{cases} = \text{const} = \dfrac{F_1}{\varrho_1} & (0 \leqslant Z \leqslant Z_1), \\ = g\bar{B}_1 V_1\left[1 - \dfrac{\gamma'}{4}(\zeta^2 - 1)^2\right] & (Z_1 \leqslant Z \leqslant Z_2), \\ = g\bar{B}_1 V_1\left[1 - \dfrac{\gamma'}{4}(\mu^2 - 1)^2 - \dfrac{l(2-l)\gamma'}{4} \times [\zeta^4 - \mu^4]\right] & (Z_2 \leqslant Z), \end{cases} \tag{22}$$

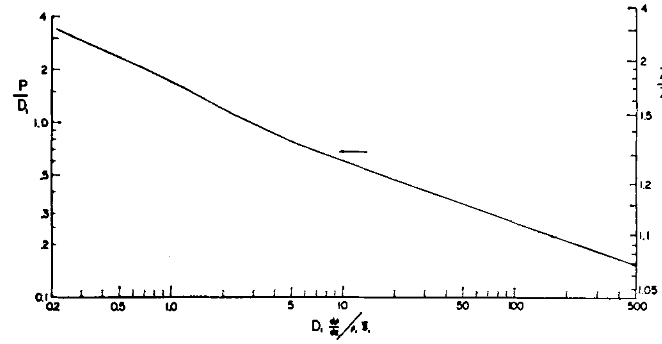

FIG. 9. The predicted penetration of a thermal in a stratification consisting of a homogeneous layer capped by a layer of constant gradient as a function of the parameter $D_1 G/g\bar{B}_1$ (equations 24, 26).

where F_1 $\bar{B}_1$ and V_1 have the same significance as previously, where we have made a partial transformation to $\zeta = Z/Z_1$ and $\mu = Z_2/Z_1$, and

$$\text{where} \qquad 2l\cdot\gamma' = \frac{Z_1 G}{g\bar{B}_1} = \frac{Z_1 \dfrac{d\bar{\varrho}_E}{dZ}}{\varrho_1 \bar{B}_1} \tag{23}$$

is the non-dimensional parameter that replaces the $\varrho_2 - \varrho_1/\varrho_1\bar{B}_1$ of the two-layer stratification.

We now complete the transformation of the variables and insert (22) into the momentum equation (3) to obtain the analogue of equation (16). At present the only interest we have here is in the penetration of the thermal into the lower layer; by putting $W = 0$ and $\zeta = \zeta_p$ it may be shown that

$$\begin{aligned} \gamma' &= 24\{3\zeta_p^4 - 8\zeta_p^2 + 6 - \zeta_p^{-4}\}^{-1} \quad (\zeta_p \leqslant \mu) \\ \gamma' &= 24\zeta_p^4\{(3\mu^8 - 8\mu^6 + 6\mu^4 - 1) + 6(\mu^2-1)^2(\zeta_p^4 - \mu^4) \\ &\quad + 3l(2-l)(\zeta_p^4-\mu^4)^2\}^{-1} \quad (\zeta_p \geqslant \mu) \end{aligned} \tag{24}$$

Taking the value $\mu = 1.3$ used previously we have calculated γ' for a range of ζ_ϱ: using the relation

$$\zeta_p - 1 = \frac{P}{Z_1} = m\cdot\frac{P}{D_1}$$

from (18) and using equation (23) we have plotted P/D_1 as a function of $(D_1 d\bar{\varrho}_E/dZ)/\varrho_1\bar{B}_1$ in Fig. 9.

Unlike the case of the two layer stratification the penetration here remains finite for all finite values of $\bar{B}_1$ and $d\varrho/dZ$. That is, however weak the stability or intense the convection the thermal is ultimately halted. From equation (22) the height of the cap of the thermal at which its average buoyancy becomes zero has also been calculated. For the range of values of the parameter $(D_1 d\bar{\varrho}_E/dZ)/\varrho_1\bar{B}_1$ from 0.2–30 the average buoyancy vanishes when the thermal has accomplished only one-half of its total penetration, the fraction falling off to one-third at $(D_1 d\bar{\varrho}_E/dZ)/\varrho_1\bar{B}_1 = 200$. Thus there is considerable 'overshoot'.

From figure 9 we can also deduce the following approximate relations:

$$\log P/D_1 \simeq \tfrac{1}{2}\log 3\left(\frac{g\bar{B}_1}{D_1 G}\right) \qquad (0.6 < P/D_1 < 3),$$

$$\log P/D_1 \simeq \tfrac{1}{3}\log 2.2\left(\frac{g\bar{B}_1}{D_1 G}\right) \qquad (0.1 < P/D_1 < 0.6).$$

Now equations (6) and (18) with $\alpha = 2.0$, $m = 0.45$ give

$$W_1^2 \approx 0.6\, g\bar{B}_1 D_1, \tag{25}$$

whence the approximate relations become

$$\left.\begin{aligned} P &\approx 2.2\frac{W_1}{G^{\frac{1}{2}}} \quad (0.6 < P/D_1 < 3), \\ P &\approx 1.6\left(\frac{W_1^2 D_1}{G}\right)^{\frac{1}{3}} \quad (0.1 < P/D_1 < 0.6). \end{aligned}\right\} \tag{26}$$

Equations (26) are here intended only as approximations useful for making rough or geophysical estimates. In this context the important result is that given a knowledge of some of the characteristics occurring in a situation of geophysical penetrative convection we can either estimate the penetration given the stability, or the stability given the penetration.

7. The convective penetration of the lower stratosphere

(a) *Discussion*

To date we have applied the predictions of the previous section to one problem only, that

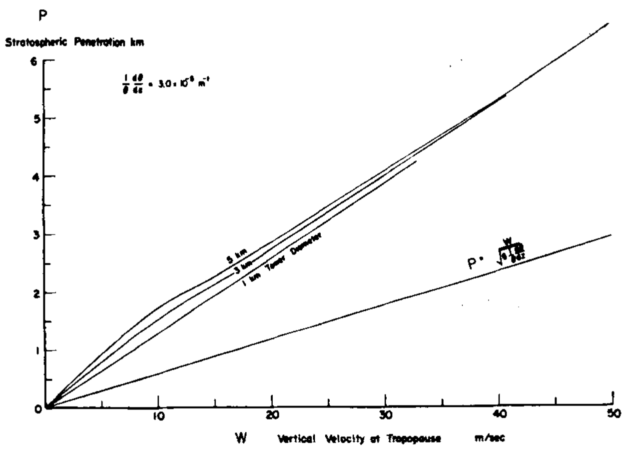

FIG. 10. The predicted penetration of the stratosphere by cumulus towers as a function of their ascent rate.

of the penetration of convective tropospheric storms into the lower stratosphere. It is fortunate that in considering the penetrative elements of these clouds, the so-called cumulus towers, we can to a first approximation entirely neglect the condensation process: in typical conditions above 250 mb the dry and saturation adiabatic lapses of temperature with height do not differ by more than 0.5°C per km. Because of the compressibility of the atmosphere the stability G is now given by

$$G = \frac{g}{\theta_1} \frac{\partial \theta}{\partial Z},$$

where θ is the potential temperature: in an isothermal atmosphere or atmosphere with constant lapse of temperature $\partial\theta/\partial Z$ and hence G are constant.

Taking $G = 3.0 \times 10^{-4}$ sec^{-2}, employing equation (25) shown by the author (1961) to be appropriate for cumulus towers in the lower troposphere, we have calculated $g\bar{B}_1$ for given D_1 and W_1 and consequently $D_1 G/g\bar{B}_1$. Entering this value as abscissa on Fig. 9, P/D_1 and hence P have been determined. In Fig. 10, P is plotted versus W_1, where W_1 now signifies the rate of rise of a cloud tower measured at or near the height of the tropopause Z_1.

As we would expect from equation (26) for moderate to large penetrations (typically $P > 3$ km) the penetration becomes directly proportional to the approach velocity; in this case we find a *penetration of 1 km for an ascent rate of 7.8 m/sec*. For $P < 3$ km the penetration depends on both velocity and diameter, increasing with both these factors.

It is of interest to compare the value derived here with previous estimates; using the "parcel" method of Refsdal (all motions adiabatic and the acceleration set equal to the buoyancy force) it is easy to show in our notation that

$$P = \frac{W}{G^{1/2}}. \tag{27}$$

This formula has been used by VONNEGUT & MOORE (1958) and MALKUS (1960) to infer W when P was known: with the value of G employed here we find *a penetration of 1 km for an ascent rate of 17 m/sec*. Equation (27) is also plotted in Fig. 10.

The difference between these results although important appears somewhat more striking than a closer examination shows. Recall that there exists a circulation in a thermal with vertical motion in the core twice the rate of advance of the cap (still observed when the cap is at height Z_1); thus the detailed treatment given here agrees with equation (27) in predicting that in *some* regions of a cloud tower vertical velocities of magnitude near 17 m/sec exist in order for a penetration of 1 km to occur.

Because mixing is permitted in the model of the thermal represented by equations 3–5 it is of interest to enquire into this correspondence with the parcel model. For small penetrations the increase in size of a thermal is small and

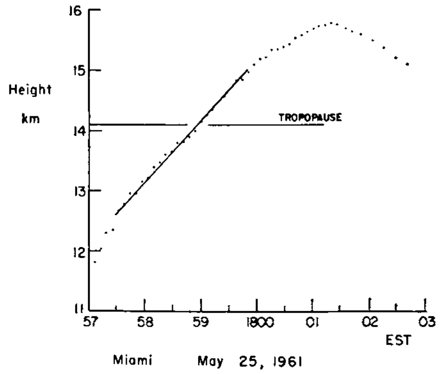

FIG. 11. The height–time relationship for tower δ of May 25, 1961. Height is measured in meters above sea level.

hence the adiabatic approximation is reasonable; for large penetrations, however, there may be a considerable increase in the mass of the thermal—for $P/D_1 = 1$, the mass increases by 100% during penetration. Now the fluid entrained consists in part of potentially warm air from the stratosphere and in part of potentially cold air from the troposphere (or the laboratory equivalents) and we find from equation (22) that their effects approximately balance, so that the adiabatic approximation for the *average* buoyancy of the thermal is still valid. This agreement seems somewhat fortuitous especially when we evaluate the buoyancy of a thermal with moderate penetration for the two layer structure (case (ii), equation (10)): there we find the adiabatic approximation a poor one. Finally we may note that whilst the use of equation (27) is justified where W signifies the maximum vertical velocity present, it does not follow that the large negative buoyancies predicted by the adiabatic model are present.

The existence of the large vertical velocities deduced from the "parcel" treatment when the stratospheric penetration is a few kilometers has long been questioned and the resolution here in their favour requires qualification. In the first place the thermal is assumed isolated and not under the influence of others; secondly, the thermal is assumed to be in an atmosphere at rest or in uniform horizontal motion. The violation of this latter condition in particular, permitting energy to be drawn from the wind field, may alter the characteristics of the penetration along lines tentatively suggested by KUETTNER (1958).

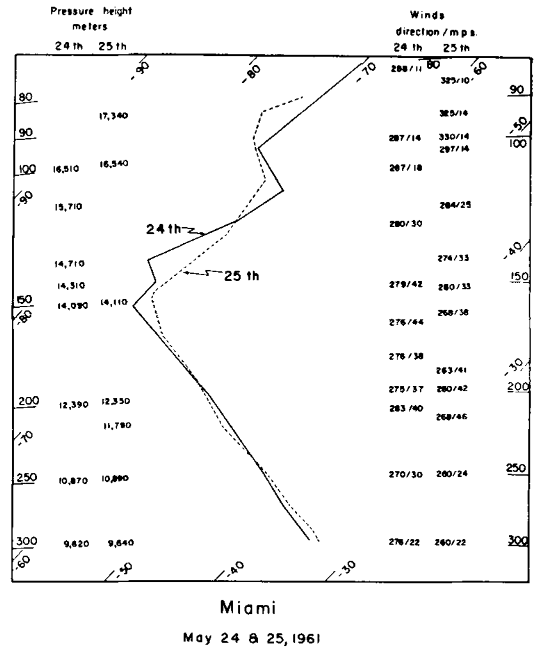

FIG. 12. Soundings at 1830 EST for Miami, Florida May 24, 25, 1961.

Thus in the final resort the validity of the results of this treatment can only be established by direct observation. Observational data bearing on this problem is presented below.

(b) *Observation*

On a recent trip to Florida in the company of F. C. Ronne the author made a combined photographic and radar study of convective cloud. The radar was a 10 cm WSR-57 unit made available for our use by the U.S. Weather Bureau. For our purposes interest centres on two evening storms of May 24–25, 1961. By careful radar study we made a number of measurements on individual cloud towers within 1 min of their reaching peak height: their slant range at peak height was then determined to an accuracy of $\pm \frac{1}{2}$ nautical mile in 25. From an analysis of concurrent time-lapse films of these clouds the tower under study was identified and by a method to be described (SAUNDERS, in preparation) its elevation was measured. Given slant range and elevation the visible cloud top was computed with an accuracy of about 2%. As has been found in numerous other estimates made with this

TABLE 1.

No.	$\frac{\varrho_2-\varrho_1}{\varrho_1 B_1}$	$\frac{P}{D_1}$	D_1cm	B_1 ($\times 10^{-3}$)	S	$\frac{\varrho_2-\varrho_1}{\varrho_1}$ ($\times 10^{-3}$)	Δcm	Pcm	P/Δ
132	$0.58 \pm .08$	∞	32.7	2.5	2.1	1.45	—	∞	—
152	$0.57 \pm .08$	3.1	17.5	3.1	2.8	1.77	1.1	54.2	49
141[a]	$0.72 \pm .10$	>2.3	25.1	11.0	2.5	7.95	1.8	>58	>32
154	$0.82 \pm .11$	$1.55 \pm .1$	24.8	5.09	2.35	4.17	1.1	38.4	35
133	$1.35 \pm .15$	$0.88 \pm .04$	35.9	1.10	2.3	1.48	1.0	31.6	32
143	$1.37 \pm .15$	$0.76 \pm .04$	28.0	6.4	2.0	8.75	0.9	21.3	22
135	$1.4 \pm .15$	$0.85 \pm .04$	30.5	2.0	2.15	2.8	1.0	25.9	26
143	$1.42 \pm .15$	$0.68 \pm .04$	30.2	5.85	2.3	8.3	1.2	20.5	17
144	$1.67 \pm .2$	$0.70 \pm .04$	32.2	4.76	2.4	7.95	1.0	22.5	22
138	$2.1 \pm .2$	$0.55 \pm .03$	27.3	2.5	2.3	5.2	1.5	15.0	10
149	$2.1 \pm .2$	$0.49 \pm .05$	18.2	4.0	2.5	8.80	1.6	8.9	5.6
151	$2.27 \pm .25$	$0.49 \pm .03$	21.5	1.94	2.5	4.41	0.6	10.5	17
130	$2.6 \pm .3$	$0.46 \pm .03$	38.0	0.78	2.4	2.02	~ 1	17.5	~ 17
137	$2.8 \pm .4$	$0.40 \pm .04$	29.2	1.97	2.5	5.53	1.2	11.7	10
155	$3.7 \pm .4$	$0.33 \pm .04$	27.0	2.1	2.2	7.79	0.9	8.9	10
157	$5.8 \pm .6$	$0.26 \pm .04$	33.4	0.97	2.0	5.60	0.7	8.7	12
102	$8.9 \pm .7$	$0.20 \pm .03$	32.7	0.75	2.65	6.72	2.0	6.5	3.3
129[b]	18.4 ± 1	0.09(?)	35.2	1.07	2.1	19.7	1.6	—	—
158	20.3 ± 2	$0.16 \pm .04$	32.4	0.73	2.3	14.8	0.8	5.2	6
161[b]	26 ± 2	0.09(?)	33.4	1.3	2.3	33.6	1.1	—	—
147[b]	26 ± 2	0.08(?)	31.8	0.76	2.5	19.8	~ 1	—	—

[a] Thermal spread on floor of tank, then returned to height Z_1; [b] Penetration measurements uncertain because of refraction; Δ is the thickness of the transition layer separating ϱ_2 and ϱ_1.

radar, the height of the visible cloud top exceeds the radar top when the tower is growing vigorously.

From the time lapse films we also evaluated the cloud height at 12-second intervals and plotted the height–time dependence (see Fig. 11 for an example): then by making a correction for the horizontal motion of the tower derived from the rate of change of azimuth and known range we evaluated the vertical velocity of the cap of the tower near the tropopause. Peak heights and ascent rates of five towers are shown in Table 2.

After this data was assembled the height of the tropopause and the stability of the lowest 2.5 km of the stratosphere were computed from radiosonde ascents made within 1 hour and 30 nautical miles of both storms (Fig. 12). We took $Z_1 = 14{,}100$ m and $G = 4.0 \times 10^{-4}$ sec^{-2} for both days. The stratospheric penetration was then calculated and found to lie between 1 and 2.5 km with a probable error of about 400 m. When the penetration is scaled by the measured ascent rate the data for all five towers is found to be consistent with the 11 m/sec per km penetration predicted from equation (26).

TABLE 2.

Date May 1961	Ident.	Radar: Range n.miles	Radar: Height m.a.s.l.	Visual: Peak m.a.s.l.	Visual: Diameter, km	Visual: Penetration, m	W_1, m/sec	W_1/P, m/sec per km
24	α	$21 \pm .5$	$14{,}000 \pm 300$	$15{,}200 \pm 600$	2.5	1100 ± 600	10 ± 4	11
25	β	$29 \pm .5$	$14{,}900 \pm 300$	$15{,}850 \pm 400$	4.5	1750 ± 400	18 ± 2	10
25	γ	$25.5 \pm .5$	$15{,}200 \pm 300$	$15{,}700 \pm 300$	3	1600 ± 400	18 ± 2	11
25	δ	$26 \pm .5$	$15{,}350 \pm 300$	$16{,}000 \pm 300$	3	1900 ± 400	18 ± 2	9.5
25	ε	$28.5 \pm .5$	$15{,}400 \pm 300$	$16{,}450 \pm 400$	5	2350 ± 500	25 ± 2	10.5

Tropopause height 14,100 m.a.s.l. (meters above sea-level)

Thus these few observations confirm the conclusions derived from equations 3–5 (more closely than is reasonable to expect) and further indicate the usefulness of the thermal theory of cumulus convection. Observations of extreme stratospheric penetrations of up to 5 km DONALDSON, CHMELA & SHACKFORD (1960), suggest a rate of ascent of visible towers of 50 m/sec with restricted internal volumes having vertical motions close to 100 m/sec. It is hoped that studies along the lines indicated here can be used to examine these extreme situations.

8. Summary

The penetrative convection of an isolated mass of buoyant fluid (thermal) into a stably stratified fluid is studied experimentally and on this basis a model for its behavior is proposed. This model employs (1) an equation of motion which balances the momentum of the thermal against the total buoyancy force acting on it; (ii) a conservation equation for the heat or salt which generates the buoyancy of the thermal; and (ii) an equation asserting a linear increase of thermal diameter with height.

These equations are then shown to rationalize data describing the behaviour of a thermal in an environment with (*a*) a neutral stratification, (*b*) a discontinuous two-layer structure, and (*c*) a constant stability throughout: they are then employed to predict the behaviour of a thermal when a neutral layer (*a*) is capped by a layer of constant stability (*c*), a situation of some geophysical interest. Given information about the amplitude of the convective processes in the neutral layer we can then estimate how far these motions penetrate into the surmounting stable layer.

As an example we have discussed the penetration of tall convective storms into the stratosphere and shown that in typical conditions a tower ascending at the rate of 10 m/sec achieves a penetration of 1 km. A limited amount of observational data is presented in support of this conclusion.

9. Acknowledgements

The work described in this paper was made possible by the support of the National Science Foundation under grant number 7368. The author also wishes to thank the U.S. Weather Bureau for support and facilities during the field trip on which the observational data was taken.

REFERENCES

DONALDSON, R. J., CHMELA, A. C., and SHACKFORD, C. R., 1960, Some behaviour patterns of New England hailstorms. Physics of Precipitation, *Geophysical Monograph No.* **5**. Amer. Geophys. Union. pp. 354–368.

KUETTNER, J. P., 1960, *Discussion to paper Giant Electrical Storms* (Vonnegut & More, loc. cit.) p. 410.

MALKUS, J. S., 1960, Recent developments in studies of penetrative convection and an application to hurricane cumulo-nimbus towers. *Cumulus Dynamics*. Pergamon Press, pp. 65–84.

MORTON, B. R., TAYLOR, G. I., and TURNER, J. S., 1956, Turbulent gravitational convection from maintained and instantaneous sources. *Proc. Roy. Soc. A*, **234**, pp. 1–23.

SAUNDERS, P. M., 1961, An observational study of cumulus. *J. Met.*, **18**, pp. 451–467.

SCORER, R. S., 1957, Experiments on convection of isolated masses of buoyant fluid. *J. Fluid Mech.*, **2**, pp. 583–594.

TURNER, J. S., 1960, Comparison between buoyant vortex rings and vortex pairs. *J. Fluid Mech.* **7**, pp. 419–432.

VONNEGUT, B., and MOORE, C. B., 1960, Giant electrical storms. *Recent Advances in Atmospheric Electricity*. Pergamon Press, pp. 399–410.

WOODWARD, E. W., 1959, The motion in and around isolated thermals. *Quart. J. Met. Soc.*, **85**, pp. 144–151.